doi:10.1016/j.jmb.2010.09.057 J. Mol. Biol. (2010) 404, 537–552

Contents lists available at www.sciencedirect.com

Journal of Molecular Biology

journal homepage: http://ees.elsevier.com.jmb

Mechanism of Fiber Assembly: Treatment of Aβ Peptide Aggregation with a Coarse-Grained United-Residue Force Field

Ana Rojas[1,2], Adam Liwo[2], Dana Browne[1] and Harold A. Scheraga[2]*

[1]*Department of Physics and Astronomy, Louisiana State University, Baton Rouge, LA 70803, USA*
[2]*Baker Laboratory of Chemistry and Chemical Biology, Cornell University, Ithaca, NY 14853-1301, USA*

Received 18 June 2010;
received in revised form
24 September 2010;
accepted 24 September 2010
Available online
1 October 2010

Edited by D. Case

Keywords:
amyloids;
Aβ peptide;
hydrophobic interactions;
molecular dynamics;
UNRES force field

The growth mechanism of β-amyloid (Aβ) peptide fibrils was studied by a physics-based coarse-grained united-residue model and molecular dynamics (MD) simulations. To identify the mechanism of monomer addition to an $A\beta_{1-40}$ fibril, we placed an unstructured monomer at a distance of 20 Å from a fibril template and allowed it to interact freely with the latter. The monomer was not biased towards fibril conformation by either the force field or the MD algorithm. With the use of a coarse-grained model with replica-exchange molecular dynamics, a longer timescale was accessible, making it possible to observe how the monomers probe different binding modes during their search for the fibril conformation. Although different assembly pathways were seen, they all follow a dock-lock mechanism with two distinct locking stages, consistent with experimental data on fibril elongation. Whereas these experiments have not been able to characterize the conformations populating the different stages, we have been able to describe these different stages explicitly by following free monomers as they dock onto a fibril template and to adopt the fibril conformation (i.e., we describe fibril elongation step by step at the molecular level). During the first stage of the assembly ("docking"), the monomer tries different conformations. After docking, the monomer is locked into the fibril through two different locking stages. In the first stage, the monomer forms hydrogen bonds with the fibril template along one of the strands in a two-stranded β-hairpin; in the second stage, hydrogen bonds are formed along the second strand, locking the monomer into the fibril structure. The data reveal a free-energy barrier separating the two locking stages. The importance of hydrophobic interactions and hydrogen bonds in the stability of the Aβ fibril structure was examined by carrying out additional canonical MD simulations of oligomers with different numbers of chains (4–16 chains), with the fibril structure as the initial conformation. The data confirm that the structures are stabilized largely by hydrophobic interactions and show that intermolecular hydrogen bonds are highly stable and contribute to the stability of the oligomers as well.

*Corresponding author.

Abbreviations used: Aβ, β-amyloid; MD, molecular dynamics; AD, Alzheimer's disease; UNRES, united residue; REMD, replica-exchange molecular dynamics; CV, concave; CX, convex; NHB, native hydrogen bond; nNHB, nonnative hydrogen bond.

Introduction

Many diseases have been associated with deposits of amyloid plaques, including Alzheimer's disease (AD), Parkinson's disease, type II diabetes, and

spongiform encephalopathies. In the particular case of AD, these plaques contain filamentous forms of a protein known as β-amyloid (Aβ) peptide.[1,2] Oligomeric forms of this protein, both fibrillar Aβ aggregates[3] and soluble nonfibrillar Aβ aggregates,[4] have been identified as the cause of AD. However, the mechanism(s) by which they may initiate the disease is still unclear.[5]

Great progress in elucidating the three-dimensional structure of amyloid fibrils has been achieved,[6–12] and we now know that amyloid fibrils from different species share a characteristic motif (the cross-β-structure) in which polypeptide chains form extended β-strands that align perpendicular to the axis of the fibril. Fibrils formed by the Alzheimer's $A\beta_{1-40}$ peptide have been studied extensively by Tycko,[9] Petkova *et al.*,[10] and Paravastu *et al.*[12] Structural models of $A\beta_{1-40}$ fibrils have been proposed based on constraints from solid-state NMR.[10,12]

Despite progress in understanding the fibrillar state of Aβ, the mechanism by which small oligomers evolve into their fibrillar form or the mechanism by which these fibrils grow is not yet well understood.[13] In the laboratory, $A\beta_{1-40}$ fibril formation takes as long as days,[14,15] and elongation proceeds by incorporating new monomers at a constant rate of approximately 0.3 μm/min (with a few milliseconds per monomer incorporated).[14] These timescales make simulations of fibril formation (or elongation) extremely challenging.

To overcome time limitation, most all-atom studies have focused on small fragments of Aβ.[16–18] Although these studies[17,18] have contributed greatly to our understanding of the transition that an unstructured monomer undergoes upon binding to a fibril, they might not reflect the full complexity of the complete $A\beta_{1-40}$ system. Implicit-solvent all-atom simulations of $A\beta_{1-40}$ elongation have been carried out;[19] however, due to their high computational cost, these simulations could not describe the assembly of a completely unstructured and unbound monomer into a fibril template. Another approach has been the use of coarse-grained models, biased towards the desired conformation,[20,21] or simplified models, in which the polypeptide chain is represented by a tube and interactions between amino acids are derived from geometry and symmetry considerations.[22] These models have the disadvantage that they might not reproduce the complexity of the true energy landscape.

In this work, we have adopted a coarse-grained united-residue (UNRES) model[23,24] to partially surmount the timescale problem. The advantage of UNRES over other coarse-grained force fields is that UNRES has been derived based on physical principles. Energy terms result from the averaging of the less important degrees of freedom of the all-atom free energy of a protein and of the solvent.[23] The force field ultimately has been parameterized to reproduce the free-energy landscape of a small training protein, which is completely different from Aβ.[25–29] Therefore, the force field is not biased towards the Aβ fibril conformation. Moreover, UNRES has been shown to be able to carry out molecular dynamics (MD) simulations of the folding of multichain systems within reasonable time, starting from completely unstructured conformations and without using any information from the native structure of these systems.[24] Therefore, UNRES has been adopted to simulate the assembly of a free monomer onto a fibril template without imposing any type of restraint on the monomer. A description of the force field,[23] as well as details of the MD implementation,[24,30,31] can be found in The UNRES Force Field and Constant Temperature Simulations (Supplementary Data).

With the UNRES model, we carried out canonical MD and replica-exchange molecular dynamics (REMD) simulations to: (a) describe the ensemble of conformations explored by the isolated monomer of $A\beta_{1-40}$; (b) analyze the stability and energetics of small oligomers of $A\beta_{1-40}$ with the structure characteristic of $A\beta_{1-40}$ fibrils and determine how their stability is related to the size of the oligomers; and (c) study the elongation process of $A\beta_{1-40}$ fibrils.

Results and Discussion

Characterizing the ensemble of isolated monomers

While oligomeric forms of Aβ adopt β-rich structures in the monomeric state, the peptide seems to adopt helical conformations.[32] Unfortunately, because Aβ has a high tendency to aggregate and eventually precipitate, it has not yet been possible to study the full-length peptide in water solution. Experiments on fragments of Aβ in water at low pH showed that the fragments have little regular structure.[33,34] For prevention of aggregation, many experiments are carried out in a mixture of water and organic solvents such as trifluoroethanol,[35,36] micellar solutions,[37,38] or hexafluoroisopropanol.[32,39] Under these conditions, the monomeric Aβ peptide shows substantial helical structure.

All-atom implicit-solvent simulations[40,41] showed that $A\beta_{39}$ adopts random-coil and helical conformations,[41] while $A\beta_{40}$ and $A\beta_{42}$ exist predominantly in two types of conformations, each one possessing significant amounts of either α-structure or β-structure.[40] All-atom explicit-solvent simulations also support the hypothesis that Aβ can adopt helical conformations as a monomer.[32]

The ability of Aβ to adopt both helical conformations and β-sheet conformations is also supported

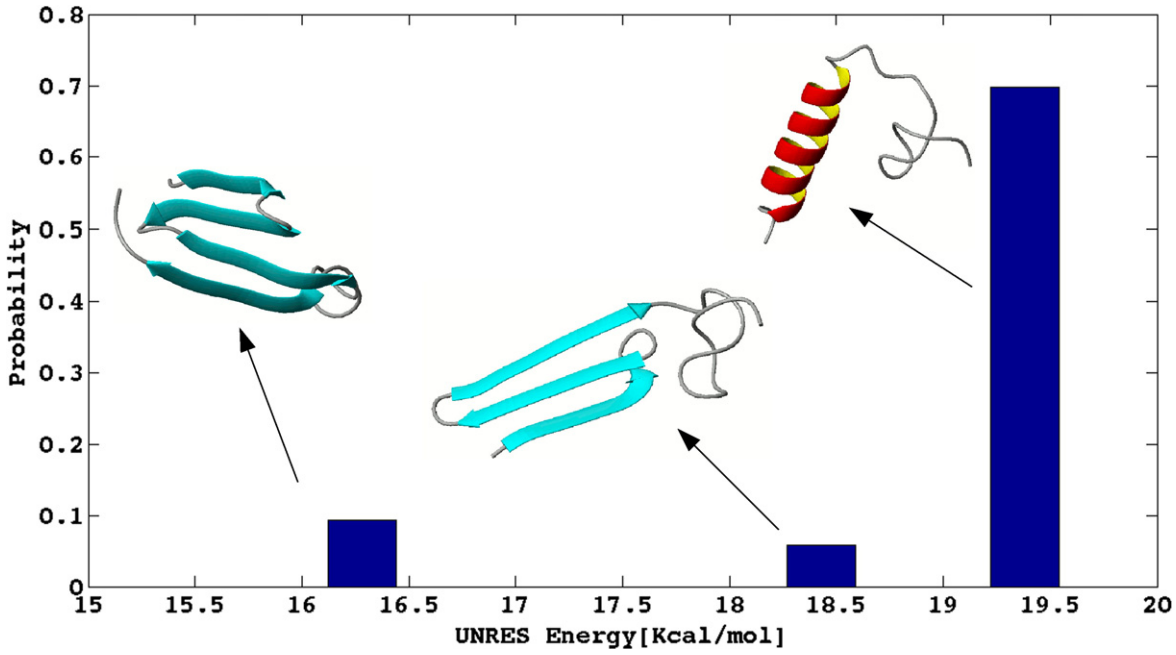

Fig. 1. The probability of occurrence of the conformations populating the three largest clusters as a function of the UNRES potential energy of the representative conformation. The representative conformation of a cluster is defined as that with the lowest RMSD from all other members of the cluster. The representative conformation for each cluster is shown, and correspondence is indicated by arrows.

by the fact that a helical intermediate has been observed during fibril assembly.[42,43] Furthermore, up to a certain degree, fibril formation accelerates with stabilization of helical conformations,[43] suggesting that the helical intermediate might facilitate the process.[42,43]

The foregoing results indicate that a model suitable for the study of Aβs should be able to capture α-helical propensity at the monomer level and the formation of oligomeric structures with high β-content. To test whether UNRES could capture the ability of monomers to adopt α-helical and β-sheet conformations, we carried out a set of 40-ns independent canonical MD simulations of an isolated monomer of $A\beta_{1-40}$ at constant temperature (for computational details, see MD Simulations of Isolated Monomers).

$A\beta_{1-40}$ populates three main clusters with α-helix or β-strand conformations

The conformations visited by the monomer were clustered based on their structures (see MD Simulations of Isolated Monomers). The three largest clusters, accounting for 69% of the conformations, were identified. These three clusters also contained the conformations with the lowest energies, as calculated with the UNRES force field. The largest of these three, containing 56.5% of the conformations, corresponds to structures with high α-helical content (see Fig. 1). The second and third largest clusters, accounting for 7.5% and 4.7% of the conformations, have β-structures. Figure 1 shows the probability of occurrence of conformations populating the three largest clusters as a function of the UNRES potential energy of each cluster (see MD Simulations of Isolated Monomers). A representative conformation for each cluster is also shown.

These results indicate that, at the monomer level, UNRES can reproduce the ability of $A\beta_{1-40}$ to adopt helical and β-strand conformations. Furthermore, the UNRES force field, being a coarse-grained one, can facilitate a study of the behavior of large oligomers—a task that remains challenging with an all-atom force field, making UNRES a very good choice for the study of Aβs.

Stability of $A\beta_{1-40}$ fibril conformation

In order to study fibril propagation, we want to determine the smallest system that can reproduce the interaction between a fibril and a free monomer. From solid-state NMR studies, we know the structure of $A\beta_{1-40}$,[9,10,12] but we do not know whether a small section of a fibril will be stable by itself or will produce the interactions of a full-length fibril in the presence of an incoming monomer. In this section, we determine the size of the system needed to reproduce these interactions.

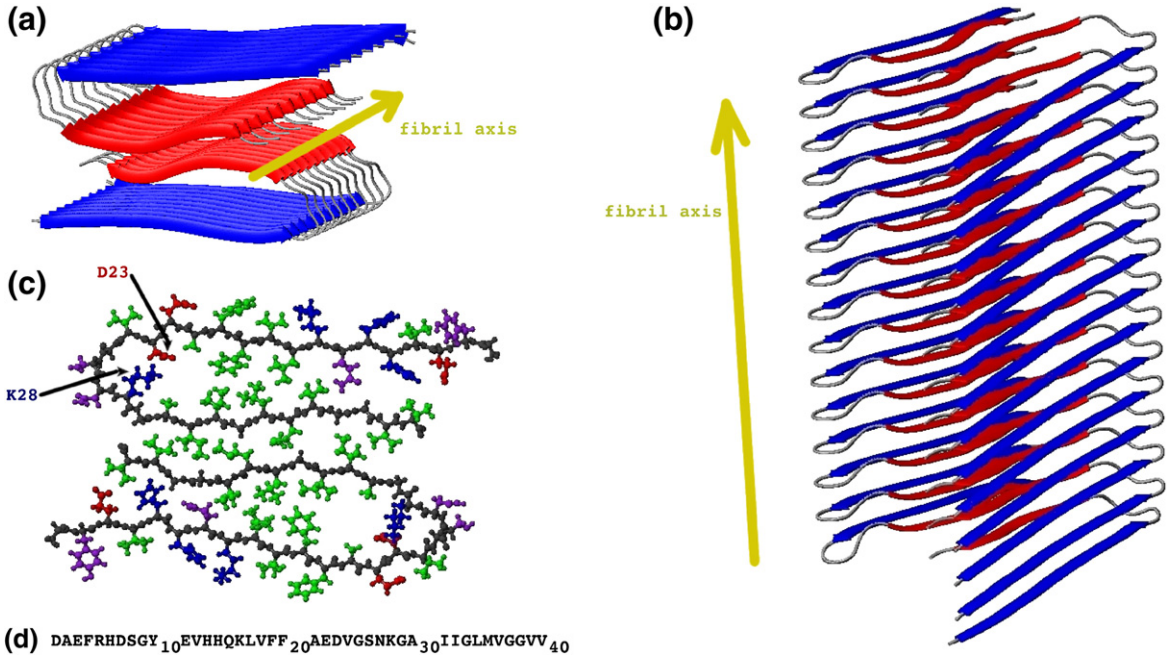

Fig. 2. Structural model of an $A\beta_{1-40}$ fibril with a striated-ribbon morphology. The figure was produced with MOLMOL,[44] based on the coordinates provided by Tycko for the structural model of Petkova *et al.*[10] Residues 1–8 are omitted from the diagram because they were conformationally disordered in the NMR model.[10] (a) Axial view and (b) side view of the fibril. The fibril axis is indicated by a dark-yellow arrow. N-terminal β-strands are shown in blue, while C-terminal β-strands are shown in red. The fibril is formed by layers of dimers lying perpendicular to the fibril axis. (c) An all-atom representation of a dimer from a fibril layer. Hydrophobic, polar, negatively charged, and positively charged side chains are shown in green, purple, red, and blue, respectively. (d) The sequence of $A\beta_{1-40}$. Only residues 9–40 were used in the simulations of oligomers.

Solid-state NMR studies[9,10,12] of $A\beta_{1-40}$ fibrils have shown that, in the fibrillar conformation, the peptide adopts the cross-β-structure (Fig. 2a).[44] Each chain adopts a hairpin-like structure (Fig. 2c) but lacks the hydrogen bonds of conventional anti-parallel β-sheets. These hairpins associate in pairs that lie on the same plane, forming the double-hairpin structures of Fig. 2c. These double-hairpin structures form interplane parallel β-sheet-like hydrogen bonds with a similar pair of hairpins in a consecutive layer.

When describing fibrillar structures, we will use the term *layer* to refer to the unit containing the dimer (Fig. 2c), which is perpendicular to the fibril axis. The term *semifilament* will be used to refer to a stack of hydrogen-bonded monomers, which are parallel with the fibril axis. According to this terminology, a fibril can be seen as formed by two parallel semifilaments or by a stack of parallel layers.

From NMR experiments,[9,10] we know that $A\beta_{1-40}$ fibrils are stabilized primarily by hydrogen bonds and hydrophobic interactions. Specifically, residues L17, F19, A21, A30, I32, L34, and V36 create a hydrophobic cluster between the β-strands in each monomer (Fig. 2c) and between the β-strands of one monomer and those of a monomer in a consecutive layer within each semifilament. The structure is stabilized further by salt bridges between oppositely charged residues D23 and K28, within the same layers or between consecutive layers.[45] At the interface of the two monomers in a given plane (Fig. 2c), the structure is stabilized by hydrophobic interactions involving residues I31, M35, and V39. In-registry intermolecular hydrogen bonds comprising residues 10–22 and 30–40 are formed between consecutive layers.[9,10]

The question on whether a small oligomer of $A\beta_{40}$ could be stable in the fibrillar conformation has been studied by computer simulations.[21,45] Buchete *et al.* used MD and all-atom force fields to study the behavior of a four-layer $A\beta_{40}$ oligomer (i.e., an eight-chain oligomer) and showed that the system was stable during a 10-ns simulation.[45] On the other hand, with a coarse-grained model, Fawzi *et al.* found that $A\beta_{1-40}$ oligomers were stable only for systems with eight layers (16 chains) or more.[21]

In order to design our simulations, we needed to answer the following questions. Will the native structure of $A\beta_{40}$ oligomers be stable with the UNRES force field? How will the stability of oligomers change when their size is changed? And,

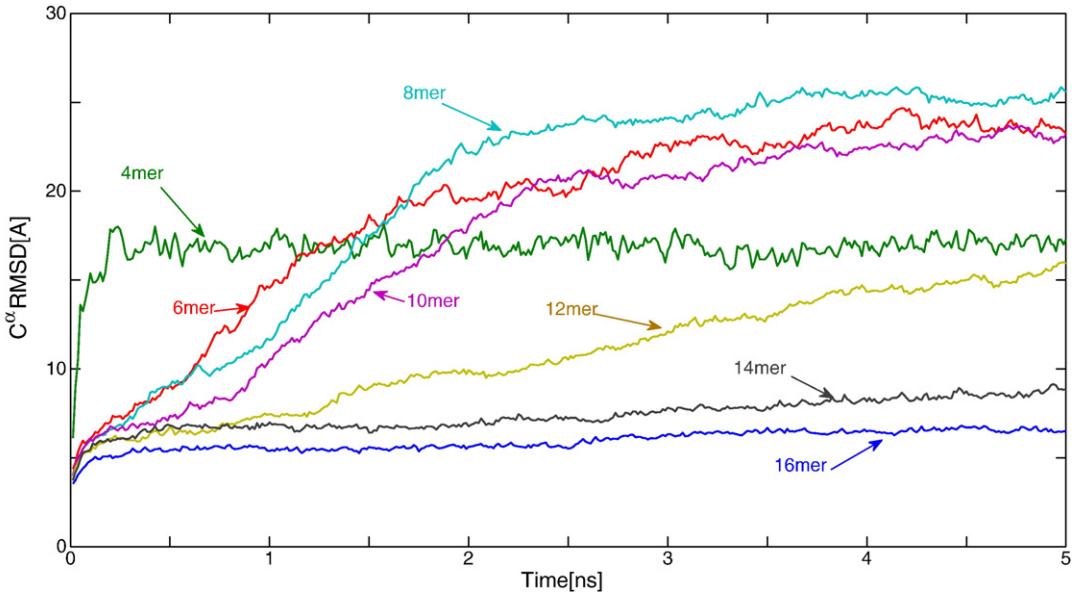

Fig. 3. Average variation of the C^{α} RMSD with respect to the initial structure during constant temperature canonical MD simulations of $A\beta_{9-40}$ oligomers with different numbers of chains per oligomer.

finally, will the interactions with free monomer change when the size of the oligomer is altered? To answer these questions, we carried out canonical MD simulations with the UNRES force field, starting from the native conformation,[10] and allowed it to fluctuate freely (see Stability of $A\beta_{9-40}$ Oligomers). Since NMR data indicated that residues 1–8 were conformationally disordered and omitted in the structural model,[10] we used the $A\beta_{9-40}$ segment (for which the coordinates are available) in our simulations.

Simulations of $A\beta_{9-40}$ oligomers with different numbers of chains

We studied systems with different numbers of layers ranging from 2 to 8 (i.e., 4–16 chains). For each system, eight independent 5-ns canonical MD trajectories were simulated at 300 K. To assess the extent of structural changes during the simulations, we measured the C^{α} root-mean-square deviation (RMSD) with respect to the initial conformation. The average RMSD (taken over all trajectories with the same size) as a function of time for different sizes is shown in Fig. 3.

From Fig. 3, it can be seen that, except for the 14-chain and 16-chain systems, the rest of the oligomers lose their initial structure during the simulation. Therefore, unless we decide to use systems as large as 14 chains, which will be too costly for simulating the free binding of monomers, we need to restrain the chains to the fibrillar conformation. We did not extend the simulations beyond 5 ns because that timescale was enough to observe the instability of small oligomers. Snapshots along the pathway of representative trajectories illustrating the behavior of the different oligomers that do not retain their fibrillar structure are included in Fig. S2 of Supplementary Data.

To find the reasons for the instability of the different oligomers and to determine whether they could still act as fibril seeds for the addition of a free monomer, we analyzed the energetics of the system. In Hydrophobic Interactions Increase Linearly with the Number of Chains, Interlayer Hydrogen Bonds Are Cooperative and Stabilize $A\beta_{9-40}$ Oligomers, and Fibril Elongation with the UNRES Force Field Will Not Involve D23-K28 Salt-Bridge Formation, we examine the three main interactions stabilizing Aβ fibrils, hydrophobic interactions, hydrogen bonds, and salt bridges.

Hydrophobic interactions increase linearly with the number of chains

Our simulations (Fig. 3) show that oligomers with 14 chains or more are stable, but smaller oligomers are not. The reason is that, as the number of layers in the oligomer increases, the size of the hydrophobic core increases as well, and nonpolar residues, especially in the center of the structure, are better buried, making the larger oligomers more stable. This becomes evident in Fig. 4a, which shows the average side-chain–side-chain energy, which in UNRES represents hydrophobic/hydrophilic interactions, averaged over the number of chains ($\langle U_{SCiSCj} \rangle$), as a function of oligomer size. As the size increases, the average contribution to U_{SCiSCj} per chain becomes larger, reaching a plateau at around 14 chains.

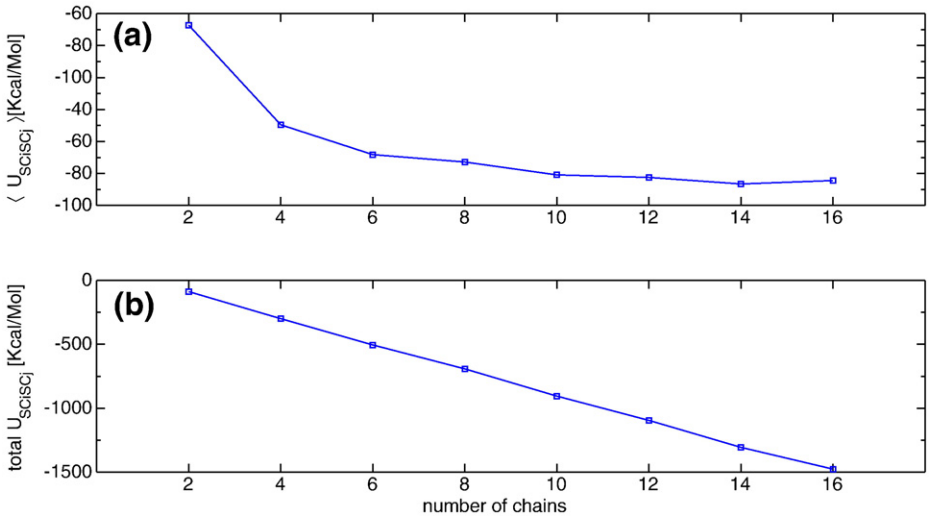

Fig. 4. (a) Average side-chain–side-chain energy per chain ($\langle U_{SCiSCj}\rangle$), and (b) the total U_{SCiSCj} energy as a function of the number of chains.

The reason for the instability of the small oligomers of $A\beta_{9-40}$ with the UNRES force field can be found in the competition between hydrophobic interactions and electrostatic interactions, the dominant contribution to which comes from the term $U_{corr}^{(3)}$.[23] In UNRES, the $U_{corr}^{(3)}$ energy term corresponds to coupling between the dipole moments of two interacting peptide groups and the geometry of the backbone around them.[23] The particular conformation adopted by $A\beta_{1-40}$ fibrils is destabilized by this term, and a larger hydrophobic core is needed to compensate for it. A more detailed discussion of this effect is included in Destabilizing Effect of the Electrostatic Interactions (Supplementary Data).

It should be noted that the behavior of $\langle U_{SCiSCj}\rangle$ does not reflect a cooperative effect. As can be seen in Fig. 4b, U_{SCiSCj} energy changes linearly with the number of layers. This means that, except for the first layer, which contributes only with intralayer hydrophobic interactions, adding a layer to a template always contributes with approximately the same U_{SCiSCj} energy, independent of the size of the systems. The edge effect, caused by the first layer not being able to hide nonpolar residues from the solvent, becomes less important as the number of layers increases, and the hydrophobic core dominates, resulting in a more stable system (for a more detailed discussion, see Linear Behavior of Hydrophobic Interactions with Respect to the Number of Chains, Supplementary Data).

The linear behavior of U_{SCiSCj} also implies that any layer in the fibrillar structure will have hydrophobic interactions with the layers adjacent to it. This means that, as far as hydrophobic contributions are concerned, we need only a one-layer system to simulate monomer–fibril interactions because the incoming monomer will interact only with the first layer at the surface of the fibril.

Interlayer hydrogen bonds are cooperative and stabilize $A\beta_{9-40}$ oligomers

Even when the secondary structure of the monomers is lost, the hydrogen bonds between consecutive layers remain intact. This is expected since the stability of hydrogen bonds along each β-sheet is enhanced by their cooperative nature,[46] and UNRES is capable of capturing this effect.[23] The hydrogen bonds play an important role in stabilizing the structure of the larger Aβ oligomers, although not in the same way as hydrophobic interactions. The fact that they make the stacking highly stable limits the conformational space available to the peptides in the stack. Being so stable, the hydrogen bonds act as restraints that restrict the conformational space of the hydrogen-bonded chains and reduce the conformational entropy of the unfolded state with respect to the folded state. The larger is the system, the more limited is the conformational space of its unfolded state and, therefore, the more stable will be the system.

We also studied the presence of cooperativity in hydrogen-bonding interactions along the direction of the fibrils. Quantum mechanical calculations of small (six to seven residues) protein fragments, which are known to form amyloid fibrils,[6,11] have shown that hydrogen-bonding interactions are cooperative for the addition of one to three layers, becoming constant for later additions.[47,48] These results suggest that hydrogen-bond cooperativity might also be present in $A\beta_{1-40}$. To test this hypothesis, we calculated the changes in UNRES hydrogen-bonding energy when adding a layer to a preexisting oligomer of n layers. This energy is obtained by computing the difference

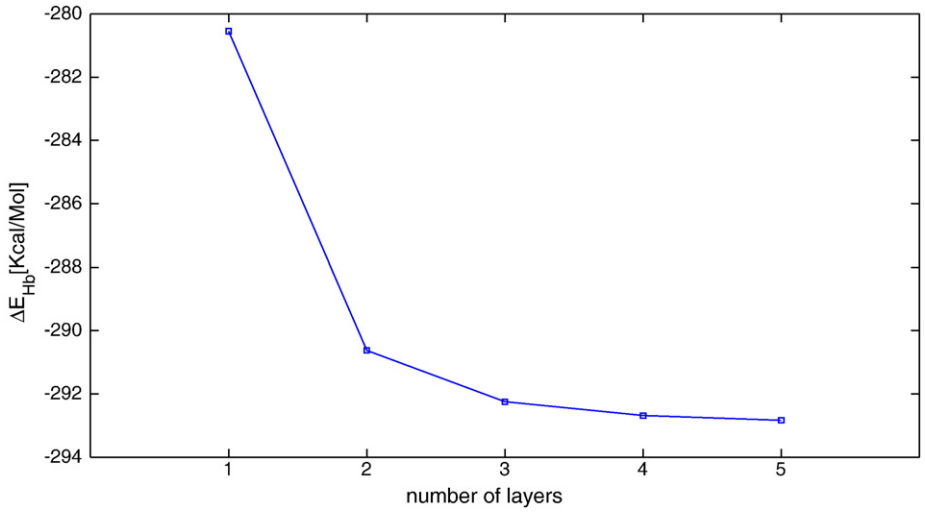

Fig. 5. Difference in the UNRES hydrogen-bonding energy ΔE_{Hb} when adding a layer to a preexisting oligomer of n layers. The $\Delta E_{Hb}(n)$ value is obtained by computing the difference between the hydrogen-bonding energy of an oligomer with n layers and the hydrogen-bonding energy of an oligomer with $n+1$ layers. $\Delta E_{Hb}(n) = E_{Hb}(n+1) - E_{Hb}(n)$.

$\Delta E_{Hb}(n)$ between the hydrogen-bonding energy of an oligomer with n layers and the hydrogen-bonding energy of an oligomer with $n+1$ layers [$\Delta E_{Hb}(n) = \Delta E_{Hb}(n+1) - E_{Hb}(n)$]. As can be seen from Fig. 5, $\Delta E_{Hb}(n)$ values become increasingly negative with the addition of the first two layers and remain almost constant for subsequent additions, in good agreement with the quantum mechanical calculations for a seven-residue peptide.[47] This result implies that, as for hydrogen-bonding contributions, we need at least a two-layer system—or perhaps even a three-layer system—to reproduce the monomer–fibril interactions. Having a larger system will contribute to the stability of the system but will not make a difference in the monomer–fibril interactions.

Fibril elongation with the UNRES force field will not involve D23-K28 salt-bridge formation

Finally, we examined the interactions between the oppositely charged residues D23 and K28, which are buried in the interior of the hydrophobic core in the NMR model, forming a salt bridge that should contribute to the stabilization of the structure.[45] However, the version of UNRES implemented in this study does not favor conformations with residues D and K in close interaction. The interactions between D23 and K28 are slightly repulsive in UNRES, helping to separate the N-terminal and C-terminal strands of the monomers. Although D23-K28 repulsive interactions are not strong enough to destabilize the structure, the absence of an attractive force between them—an interaction that is important in the formation and stability of real $A\beta_{1-40}$ fibrils[10,1545]—hampers the stability of the oligomers. This problem is addressed by introducing a new physics-based side-chain–side-chain potential energy into UNRES (work in progress).

Experimental studies suggest that the formation of the D23-K28 salt bridge might be the rate-limiting step in $A\beta_{1-40}$ fibril formation and elongation.[15] Simulations of Aβ monomers showed that D23 and K28 are initially solvated and need to overcome a high desolvation barrier to form a salt bridge,[49] supporting the hypothesis that the formation of the salt bridge is the rate-limiting step and that, therefore, it must be an early event.[49] But it is also possible that other interactions guide the peptide towards the hairpin-like conformation and facilitate the formation of the salt bridge, which, once formed, further stabilizes the structure. The repulsive interaction between D23 and K28 with the UNRES force field will, in a sense, account for solvation penalty. If the formation of the salt bridge in the monomer is a necessary step for fibril elongation, we would not see the event. As we describe in The Same Binding Mechanism Is Observed at Both Ends of the Template, Monomer Addition Following a Dock-Lock Mechanism with Two Distinct Locking States, The Second Locking Step Is Highly Cooperative, Binding Mechanism Does Not Change with Template Size, and Simulations Do Not Show a Preferred Fibril End for Monomer Binding, we do see fibril elongation with UNRES.

Fibril elongation

The polymerization process of Aβ fibril formation[50–52] is characterized by a lag phase, during which a critical nucleus (seed) is formed, followed by a faster growth phase, during which free monomers are incorporated into the seed.[51] *In*

vitro experiments have estimated that amyloid fibril formation takes days,[15] making computer simulations of the assembly of monomers into fibrils prohibited, even with a coarse-grained approach. However, the lag phase can be bypassed if a preformed seed is introduced.[15,51] There is evidence suggesting that fibrils grow by the addition of monomers one at a time,[53] and that the monomers adopt the conformation of the seed, propagating its structure.[54] Based on this information, we focused our studies on the process of the addition of monomers onto a fibril one at a time.

It has been proposed that the addition of monomers onto $A\beta_{1-40}$ fibrils follows a two-state "dock-lock" mechanism.[55,56] In the initial stage, the monomer is docked onto the fibrils, but it can easily dissociate; in the second stage, the monomer is locked into the fibril (i.e., it will rarely dissociate). Studies of the deposition of $A\beta_{1-40}$ monomers onto AD brain tissues and synthetic amyloid fibrils[55] identified the transition between the docked state and the locked state as the rate-limiting step. Results from a more recent experiment[56] further revealed a more complex mechanism with two different locked states, with the latest having an even slower dissociation rate (i.e., both locked states are very stable, but the final state has the highest stability). Although a mechanism has been proposed,[56] it has not yet been possible to obtain a detailed description of the conformations populating the assembly states.

We studied fibril elongation with the UNRES force field using the structural model of Petkova *et al.* as fibril template.[10] Simulating fibrils of real size would be extremely costly, even with a coarse-grained model. Based on the simulations reported in Simulations of $A\beta_{9-40}$ Oligomers with Different Numbers of Chains, a two-layer (four-chain) oligomer was the smallest system that could reasonably reproduce monomer–fibril interactions. Hence, we used templates of four, six, and seven chains (i.e., 2, 3, and 3 1/2 layers). From our studies of the stability of oligomers (Simulations of $A\beta_{9-40}$ Oligomers with Different Numbers of Chains), we knew that the template structures of these sizes were not stable with UNRES. Larger templates (14 chains or more) were stable, but it would have been computationally too expensive to use such systems for the simulation of monomer addition. This problem was surmounted by adding a term to the potential energy that stabilized the fibrillar conformation (for details about this energy term, see Fibril Elongation), making the smaller templates stable as well. This energy term was applied to the chains of the fibril template, but not to the free monomer.

Preliminary simulations (data not shown) had shown that the monomer can easily become trapped in conformations with a number of energetically favorable contacts that—although not as stable as the fibrillar conformation (referred to as native here)—take a long time to dissociate. To help overcome these situations with minimum intrusion, we used REMD with a short range of temperatures (between 280 and 320 K; for details about the implementation, see Fibril Elongation). Because the temperature of replicas changes during REMD simulation, the trajectories are disturbed, and the time evolution of the replicas does not reproduce folding pathways at constant temperature but gives a reasonable description of the order of events during folding.[57] REMD has been used to study the folding process of proteins and RNA,[57–62] and different methods have been developed to obtain kinetic information from REMD simulations.[59,62,63] However, in our work, we describe only the sequence of events, and we do not attempt to make estimates of transition rates between those events or any other kinetic information.

The same binding mechanism is observed at both ends of the template

The β-strands in the fibril do not lie exactly in a plane (see Fig. 6), but the N-terminal strands are more exposed at one of the ends (bottom end in Fig. 6). Because of this asymmetry, it has been suggested that Aβ fibrils might grow in a unidirectional fashion.[19,21] Following the terminology adopted by Takeda and Klimov,[19] we refer to the exposed N-terminus as the concave (CV) end, and we refer to the exposed C-terminus as the convex (CX) end. To test whether UNRES would reflect a preferred direction of growth, we carried out two sets of REMD simulations with the monomer in an extended conformation at a distance of 20 Å from the surface of the template, differing only in the initial position of the monomer (i.e., facing either the CV end or the CX end of the fibril) (see Fig. 6). For each set, we simulated 120 REMD trajectories that are 20 ns long.

We found the same pattern in the binding mechanism at both the CV end and the CX end of the template. Snapshots from two trajectories leading to successful monomer addition for a two-layer template are shown in Fig. 7 (starting at the CV end) and Fig. 8 (starting at the CX end). In Fig. 7, the first snapshot ($t = 0.76$ ns) shows the monomer before docking onto the template. As expected from our simulations of Aβ monomers, at this point, the monomer adopts conformations with significant α-helical content. At $t = 2.62$ ns, the monomer has bound to the template at the wrong (anti-parallel) orientation. At $t = 4.77$ ns, the monomer is free again. At $t = 6.89$ ns, it attempts to bind again in a nonnative conformation. Further reorientation leads to the conformation shown at $t = 13.01$ ns, with several native hydrogen bonds (NHBs) along the C-terminal strand. Finally, the N-terminal strand follows and also makes NHBs, locking the monomer in the fibrillar conformation (snapshot at $t = 20$ ns). Figure

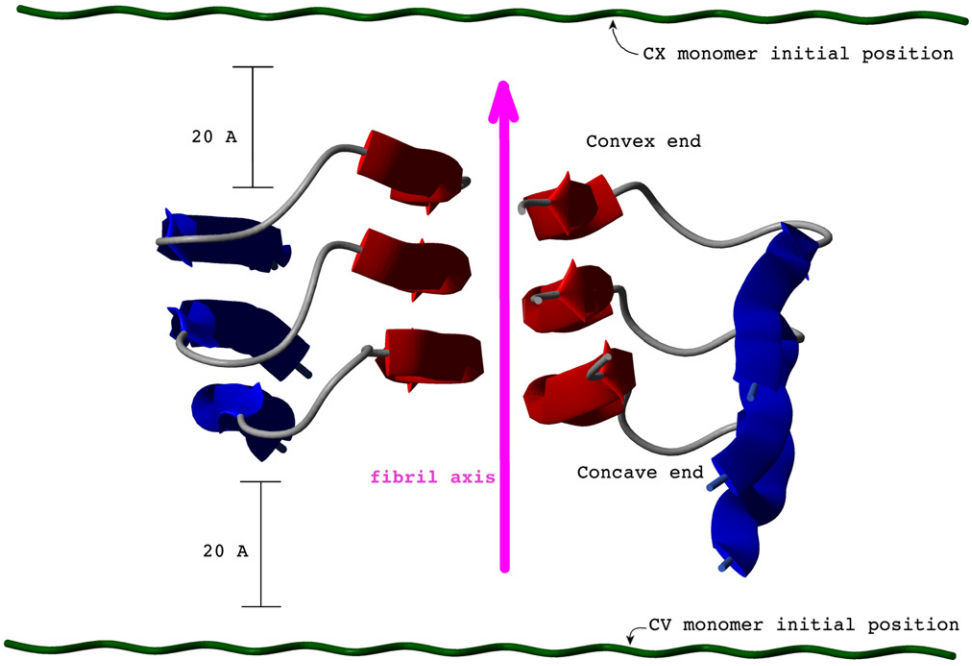

Fig. 6. Structural representation of an $A\beta_{1-40}$ fibril. A magenta arrow indicates the direction of the fibril axis. Only three planes along the axis are shown. Due to the asymmetry of the structure at the CX end, the C-terminal strands (red) are more exposed than the N-terminal strands (blue). The two different initial positions (at the CV and CX ends) of the free monomer (dark green) are shown. In both initial conformations, the monomer is extended and positioned 20 Å away from the closest fibril end.

8 shows a similar mechanism for a trajectory starting at the CX end. Initially, the monomer attempts to form nonnative conformations ($t = 0.27$ ns and $t = 1.45$ ns) that are later disrupted ($t = 3.76$ ns). Native binding starts with the assembly of its N-terminus ($t = 16.75$ ns) and later propagates towards its C-terminus ($t = 20$ ns).

Monomer addition following a dock-lock mechanism with two distinct locking states

We now look closely at the hydrogen bonds formed between the monomer and the template, along the folding trajectories shown in Figs. 7 and 8. We adopted the following criteria to classify the hydrogen bonds: a hydrogen bond between peptide groups with indices i and j was considered native if $|i-j| \leq 3$, and nonnative otherwise. Figures 9a and b show the number of NHBs and the number of nonnative hydrogen bonds (nNHBs) as a function of time for the trajectories shown in Figs. 7 and 8, respectively. For both trajectories, we can distinguish three stages in the dock-lock mechanism. During the first (docking) stage, very few NHBs are formed. The conformations adopted during this first stage are not very stable, and the monomer binds and unbinds several times (reflected in NHB and nNHB rising and going back to zero several times). In the second stage (starting at ≈10 ns in Fig. 9a and at ≈6.5 ns in Fig. 9b), which corresponds to the first locking state, the monomer makes several NHBs (NHB ≈10), locking only one of the strands, while the other strand is still free to move. The last stage corresponds to the second locking state (starting at ≈18 ns in Fig. 9a and at ≈19 ns in Fig. 9b). During this stage, the free strand makes the remaining NHBs, and the monomer is fully locked in the fibrillar conformation. Once the monomer is locked into this conformation, it can itself serve as a template for subsequent monomer additions.

This assembly mechanism is consistent with the results obtained from experiments of Aβ monomer deposition.[55,56] We have identified a docking stage and, more remarkably, the two different locking stages. From our simulations, it becomes evident that the first locking stage is a necessary step that, by locking one of the strands, limits the conformational space available to the free strand and facilitates the assembly of the rest of the peptide.

Nguyen *et al.* studied the elongation of fibrils formed by the $A\beta_{16-22}$ fragment.[16] Interestingly, the authors found that the monomers bind by a dock-lock mechanism. However, presumably because this fragment assembles with a much simpler architecture, lacking the hairpin present in $A\beta_{1-40}$, they saw a single locking stage. Our simulations show that $A\beta_{1-40}$ has a more complex mechanism, with the

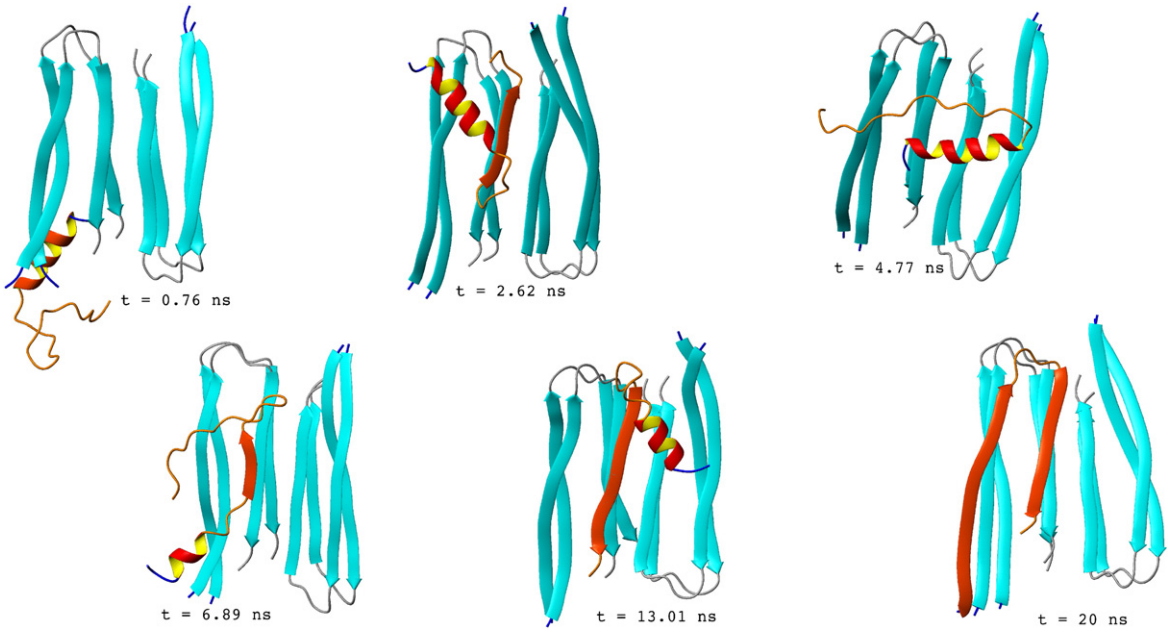

Fig. 7. Selected snapshots along a representative trajectory of a monomer binding to a four-chain fibril. The monomer is initially placed in the extended conformation and positioned 20 Å away from the CV end of the template. The snapshot at $t = 0.76$ ns shows the monomer before docking onto the fibril in a conformation with significant α-helical content. At $t = 2.62$, the monomer binds, forming an anti-parallel β-strand along the C-terminus, while the N-terminus forms an α-helix. At $t = 4.77$ ns, the monomer is again free from the template. At $t = 6.89$ ns, the monomer attempts to bind again, but the conformation is still nonnative. The monomer rearranges its position; at $t = 13.01$ ns, its C-terminus has bound with the native conformation, with the α-helix along the N-terminus still present. The α-helix unfolds and the N-terminus also binds with the native conformation, locking the monomer into the fibrillar conformation, as shown in the snapshot at $t = 20$ ns.

docking stage followed by two different locking stages.

The second locking step is highly cooperative

In the second locking stage, once the still-free strand makes one or two NHBs, these bonds quickly propagate along the rest of the strand. This is shown in Fig. 9a and b as the abrupt rise in NHB by the end of the simulation. It is also seen as a scarcely populated region between the native basin (at ≈26 NHB) and the region below 20 NHB in Fig. S4 of Supplementary Data. This behavior indicates cooperative binding. This cooperative binding has also been observed in simulations of the assembly of Aβ fragments.[17] However, these small fragments show a single locking stage. This single stage is similar to the second locking stage in $A\beta_{1-40}$ binding.

Binding mechanism does not change with template size

The larger systems with six-chain and seven-chain templates showed the same dock-lock mechanism as the four-chain templates. Here, the two locking states can also be distinguished, with the first one corresponding to the native binding of one of the strands and with the final locking state corresponding to the native binding of the second strand. Figures S5 and S6 of Supplementary Data show examples of trajectories for the six-chain and seven-chain templates.

Simulations do not show a preferred fibril end for monomer binding

We adopted the following criteria to determine whether a trajectory resulted in fibril elongation. If, at the end of the simulation, the monomer has no hydrogen bonds with any of the chains in the template, it is considered undocked. If it has formed less than 10 NHBs, it is considered a nonnative addition. If it has formed more than 10 but less than 20 NHBs, we consider it a half addition. Finally, if it has formed at least 20 NHBs with any of the chains on the fibril, we consider it a full addition. It should be noted that a half addition corresponds to a monomer in the first locking stage, and that a full addition corresponds to a monomer in the second locking stage. The numbers of undocked, nonnative, half, and full additions are listed in Table 1.

The data show that binding can occur at both ends of the fibril (CV or CX). It is interesting to note that, on several occasions, binding occurred at the opposite

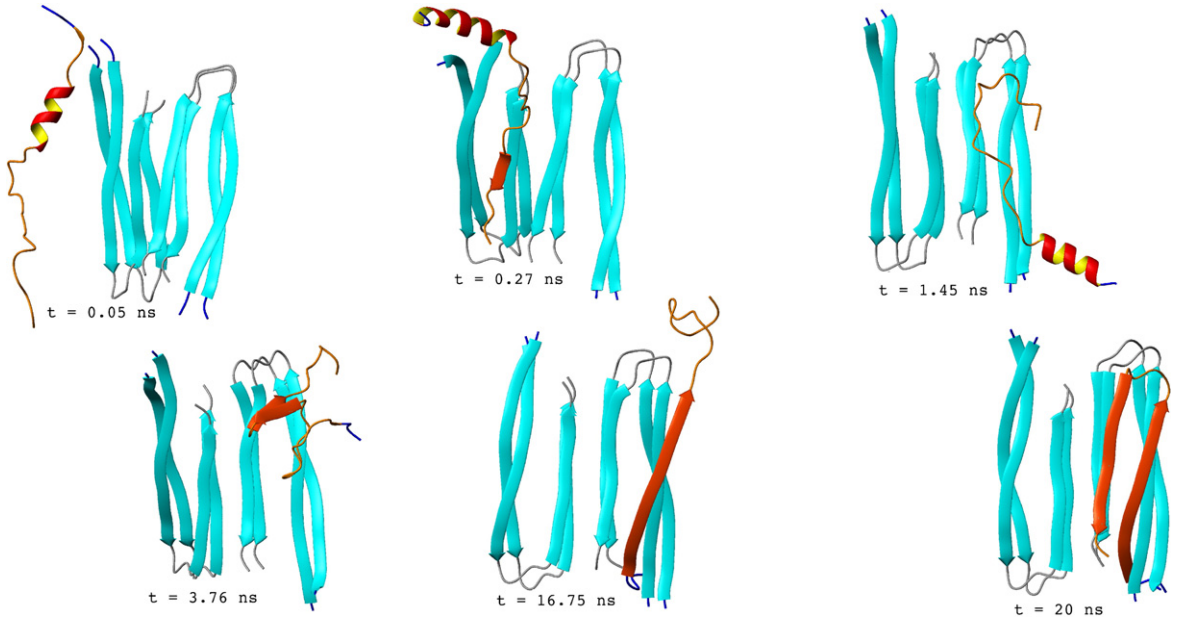

Fig. 8. Same as Fig. 7, except that the monomer is initially placed in the extended conformation and positioned 20 Å away from the CX end of the fibril. The snapshot at $t = 0.05$ ns shows the monomer before docking onto the fibril in a conformation with a certain α-helical content. The monomer makes several attempts to bind ($t = 0.27$ ns, $t = 1.45$ ns, and $t = 3.76$ ns), but none of these conformations is native, and the binding is disrupted. Native binding starts with the assembly of the N-terminal strand ($t = 16.75$ ns). The C-terminal strand follows, locking the monomer into the fibrillar conformation, as shown in the snapshot at $t = 20$ ns.

end of the fibril (i.e., a monomer initially facing the CV end could bind to the CX end, and vice versa). The numbers of full addition, half addition, and nonnative binding on the opposite end are indicated between parentheses. Although our data show a slightly larger number of half and full additions to the CV end than to the CX end, the numbers are too small to arrive at any conclusion about preferences at the ends. However, it is important to note that monomers can bind to both ends of the fibril.

Conclusions

A coarse-grained model (UNRES) has been used to study the stability of $A\beta_{9-40}$ oligomers and the process of fibril growth. Using this approach, we successfully simulated the assembly of free monomers into fibril templates, providing insight into the conformational changes leading to Aβ fibril propagation.

Regarding the stability of oligomers, we found that hydrophobic interactions play an important role in stabilizing the structures, and that these interactions become more important as the size of the oligomer increases, approaching their maximum values at around 16 chains. However, taking into account certain limitations of the force field, we conclude that oligomers smaller than 16 chains might also be stable in the fibrillar conformation.

Our results also showed that the hydrogen bonds (formed between chains in consecutive layers) are extremely stable. These hydrogen bonds act as restraints that reduce the conformational entropy of the unfolded state by limiting the conformations that the hydrogen-bonded chains can adopt, thereby increasing the stability of the folded state. For larger systems, this effect also becomes more important because more hydrogen-bonded layers will have less energetically favorable states available.

Regarding the hydrogen bonds between consecutive layers, we also studied the increase in their stability upon the addition of a new layer to a preformed oligomer. This was performed by computing the differences in hydrogen-bonding energy between oligomers of different sizes. The results indicate the presence of cooperativity in interlayer hydrogen bonds upon the addition of one to three layers. For further additions, energy change becomes constant. The result is in agreement with classical and quantum mechanical calculations with a seven-amino-acid fragment of a fibril-forming peptide from the yeast prion Sup35.[47]

Fibril elongation was studied by allowing a free monomer to interact with a fibril template. The simulations produced trajectories leading to nonnative and native bindings (native means that the monomer binds, adopting the same conformation as the other chains in the template). By studying those

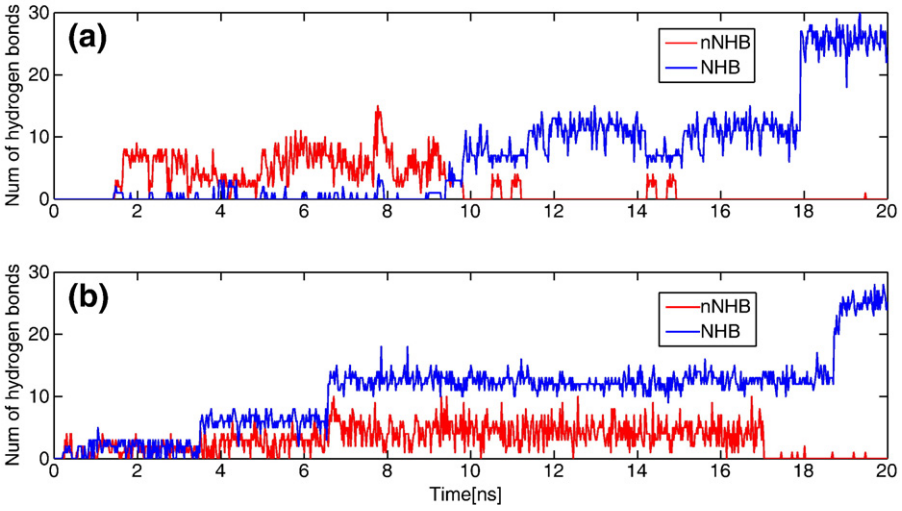

Fig. 9. The number of NHBs and the number of nNHBs between monomer and template during a trajectory leading to a full addition starting from the CV end (a) and the CX end (b).

trajectories that led to native binding, we observed that they followed a common dock-lock mechanism. During the docking stage, the monomer interacts with the template, often making nNHBs that later break. The second stage (locking) can be further divided into two consecutive steps. First, the monomer makes NHBs along one of the β-strands in the template; at this point, half of the peptide is bound to the template, while the other end can move freely. The final locking step is the native binding of the free end. This final step was highly cooperative, as indicated by the fact that, once one or two NHBs are formed between the free end and the template, these hydrogen bonds quickly propagate along the rest of the peptide. This final step locks the monomer into the fibril template. Experiments on monomer deposition[56] have indicated the presence of two locking states; however, these experiments could not describe the conformations populating these two states. Based on our simulations, we have proposed a description of this mechanism at the molecular level.

Table 1. Summary of the final conformations obtained from 120 REMD simulations

	4-mer+1		6-mer+1	7-mer+1
	From CV end[a]	From CX end[b]	From CX end[c]	From CX end[d]
Full additions[e]	2 (0)	1 (0)	1 (1)	1 (0)
Half additions[f]	14 (1)	12 (4)	6 (0)	2 (1)
Nonnative binding[g]	104(13)	107(29)	106(24)	91(11)
Undocked monomers[h]	0	0	7	26

The numbers of full addition, half addition, and nonnative binding on the opposite end are indicated between parentheses.

[a] The number of trajectories that resulted in full additions, half additions, nonnative binding, or undocked monomers for a four-chain template with the monomer initially positioned facing the CV end.

[b] The number of trajectories that resulted in full additions, half additions, nonnative binding, or undocked monomers for a four-chain template with the monomer initially positioned facing the CX end.

[c] The number of trajectories that resulted in full additions, half additions, nonnative binding, or undocked monomers for a six-chain template with the monomer initially positioned facing the CX end.

[d] The number of trajectories that resulted in full additions, half additions, nonnative binding, or undocked monomers for a seven-chain template with the monomer initially positioned facing the CX end.

[e] Trajectories were classified as full additions if, by the end of the simulation, the monomer has formed at least 20 NHBs with any of the chains on the template.

[f] Trajectories were classified as half additions if, by the end of the simulation, the monomer has formed more than 10 but less than 20 NHBs.

[g] Trajectories were classified as nonnative if, by the end of the simulation, the monomer has formed less than 10 NHBs.

[h] Trajectories were classified as undocked if, by the end of the simulation, the monomer has not formed hydrogen bonds with any of the chains in the template.

Materials and Methods

MD simulations of isolated monomers

Forty independent canonical MD simulations of monomers were carried out at a constant temperature of 300 K (held constant with a Berendsen thermostat),[64] as described in previous work.[24] The simulations were started with the monomer in the extended conformation. The monomer was allowed to equilibrate for 20 ns. The following 20 ns were then used to analyze the structures explored by the system. For each of the 40 independent trajectories, conformations were stored every 150,000 steps, providing 1200 conformations among all the trajectories. These 1200 conformations were clustered into families by the minimal tree algorithm[65,66] based on C^{α} RMSD distances between conformations. A 5-Å RMSD clustering criterion was used. Representative conformations from the three largest clusters (accounting for 69% of the conformations) are shown in Fig. 1. The UNRES energy of a cluster is calculated as that of the conformation with the lowest energy in the cluster.

Stability of $A\beta_{9-40}$ oligomers

The canonical MD simulations of $A\beta_{9-40}$ oligomers were carried out at 300 K using the Berendsen thermostat,[24,64] and the initial conformation was that of the structural model of Petkova *et al.* shown in Fig. 2.[10] The systems simulated were oligomers with an even number of chains (2, 4, 6, etc., i.e., complete layers) from 4 to 16 chains. The energies of these conformations were first minimized by carrying out 50-ps restrained canonical MD simulations (for details on restraints used, see Fibril Elongation), after which the system was allowed to evolve freely for 5 ns.

Fibril elongation

Fibril elongation was examined by simulating the interaction between a monomer and a fibril template. The fibril template was composed of four, six, or seven chains, with the conformation of the structural model of Petkova *et al.*[10] Since systems of such sizes (four to seven chains) are not stable with the version of the UNRES force field used here, an additional term, U_{Restr}, was added to it to restrain the template to the fibrillar conformation. The energy is given by Eq. (1):

$$U_{\mathrm{Restr}} = w_{\mathrm{Restr}} \sum_{l} [Q(l)-1]^2 \qquad (1)$$

where the index l runs over all of the segments being restrained, w_{Restr} is the weight of the term (set at 5×10^4 kcal/mol), and $Q(l)$ is given by Eq. (2):

$$Q(l) = \frac{1}{N_{\mathrm{dist}_l}} \left[\sum_{i,j} exp\left[-\frac{1}{2} \left(d_{i,j} - d_{i,j}^{\mathrm{nat}} \right)^2 \right] \right] \qquad (2)$$

where $d_{i,j}$ and $d_{i,j}^{\mathrm{nat}}$ are the current and native distances between the C^{α} atoms from amino acids i and j, and N_{dist_l} is the total number of distances in segment l. Two types of segments were considered: intrachain and interchain. For intrachain segments, the indices i and j were run over all of the amino acids in the chain, with $i<j$. Interchain segments were considered between adjacent chains (i.e., between chain n and chain $n+1$ or chain $n+2$). For interchain segments, the indices i and j were run over all of the amino acids in the corresponding chains.

For the simulations of fibril elongation, we used REMD.[67,68] For each system, we had 120 independent trajectories starting from the same initial conformation but at different temperatures ranging between 280 and 320 K, at intervals of 10 K. Exchanges were attempted every 20,000 steps, and each simulation was run for 20 ns. Between exchanges, the temperature was held constant with the Berendsen thermostat.[24,64] For templates consisting of six and seven chains, the monomer was initially placed at the CX end of the fibril in the extended conformation and 20 Å away from the end of the fibril. For the four-chain templates, two sets of 120 trajectories were simulated, with the monomer initially 20 Å away from the CV and CX ends, respectively.

Acknowledgements

This work was supported by the National Institutes of Health (GM-14312), the National Science Foundation (MCB05-41633), and the CCT Graduate Assistantship Program from Louisiana State University. This research was conducted using the resources of (a) our 616-processor Beowulf cluster at the Baker Laboratory of Chemistry, Cornell University; (b) the National Science Foundation Terascale Computing System at the Pittsburgh Supercomputer Center; (c) the Informatics Center of the Metropolitan Academic Network (IC MAN) in Gdańsk; and (d) the Center for Computation and Technology at Louisiana State University. We thank Dr. Robert Tycko for providing the atomic coordinates for the $A\beta_{1-40}$ structural model.

Supplementary Data

Supplementary data to this article can be found online at doi:10.1016/j.jmb.2010.09.057

References

1. Masters, C. L., Simms, G., Weinman, N. A., Multhaup, G., McDonald, B. L. & Beyreuther, K. (1985). Amyloid plaque core protein in Alzheimer disease and Down syndrome. *Proc. Natl Acad. Sci. USA*, **82**, 4245–4249.
2. Selkoe, D. (1991). The molecular pathology of Alzheimer's disease. *Neuron*, **6**, 487–498.
3. Lorenzo, A., Yuan, M., Zhang, Z., Paganetti, P., Sturchler-Pierrat, C., Staufenbiel, M. *et al.* (2000). Amyloid β interacts with the amyloid precursor protein: a potential toxic mechanism in Alzheimer's disease. *Nat. Neurosci.* **3**, 460–464.

4. Walsh, D., Klyubin, I., Fadeeva, J., Cullen, W., Anwyl, R. & Wolfe, M. (2002). Naturally secreted oligomers of amyloid beta protein potently inhibit hippocampal long-term potentiation *in vivo*. *Nature*, **416**, 535–539.
5. Yankner, B. & Lu, T. (2009). Amyloid β-protein toxicity and the pathogenesis of Alzheimer disease. *J. Biol. Chem.* **284**, 4755.
6. Nelson, R., Sawaya, M., Balbirnie, M., Madsen, A., Riekel, C., Grothe, R. & Eisenberg, D. (2005). Structure of the cross-β spine of amyloid-like fibrils. *Nature*, **435**, 773–778.
7. Ritter, C., Maddelein, M., Siemer, A., Luhrs, T., Ernst, M., Meier, B. *et al.* (2005). Correlation of structural elements and infectivity of the het-s prion. *Nature*, **435**, 844–848.
8. Makin, O. S., Atkins, E., Sikorski, P., Johansson, J. & Serpell, L. C. (2005). Molecular basis for amyloid fibril formation and stability. *Proc. Natl Acad. Sci. USA*, **102**, 315–320.
9. Tycko, R. (2006). Molecular structure of amyloid fibrils: insights from solid-state NMR. *Q. Rev. Biophys.* **39**, 1–55.
10. Petkova, A. T., Yau, W. -M. & Tycko, R. (2006). Experimental constraints on quaternary structure in Alzheimer's amyloid fibrils. *Biochemistry*, **45**, 498–512.
11. Sawaya, M., Sambashivan, S., Nelson, R., Ivanova, M., Sievers, S., Apostol, M. *et al.* (2007). Atomic structures of amyloid cross-β spines reveal varied steric zippers. *Nature*, **447**, 453–457.
12. Paravastu, A. K., Leapman, R. D., Yau, W. M. & Tycko, R. (2008). Molecular structural basis for polymorphism in Alzheimer's β-amyloid fibrils. *Proc. Natl Acad. Sci. USA*, **105**, 18349–18354.
13. Chimon, S., Shaibat, M. A., Jones, C. R., Calero, D. C., Aizezi, B. & Ishii, Y. (2007). Evidence of fibril-like β-sheet structures in a neurotoxic amyloid intermediate of Alzheimer's β-amyloid. *Nat. Struct. Mol. Biol.* **14**, 1157–1164.
14. Ban, T., Hoshino, M., Takahashi, S., Hamada, D., Hasegawa, K., Naiki, H. & Goto, Y. (2004). Direct observation of Aβ amyloid fibril growth and inhibition. *J. Mol. Biol.* **344**, 757–767.
15. Sciarretta, K., Gordon, D., Petkova, A., Tycko, R. & Meredith, S. (2005). $A\beta_{40}$-lactam(D23/K28) models a conformation highly favorable for nucleation of amyloid. *Biochemistry*, **44**, 6003–6014.
16. Nguyen, P. H., Li, M. S., Stock, G., Straub, J. E. & Thirumalai, D. (2007). Monomer adds to preformed structured oligomers of Aβ-peptides by a two-stage dock-lock mechanism. *Proc. Natl Acad. Sci. USA*, **104**, 111–116.
17. Reddy, G., Straub, J. E. & Thirumalai, D. (2009). Dynamics of locking of peptides onto growing amyloid fibrils. *Proc. Natl Acad. Sci. USA*, **106**, 11948–11953.
18. O'Brien, E., Okamoto, Y., Straub, J., Brooks, B. & Thirumalai, D. (2009). Thermodynamic perspective on the dock-lock growth mechanism of amyloid fibrils. *J. Phys. Chem. B*, **113**, 14421–14430.
19. Takeda, T. & Klimov, D. (2009). Replica exchange simulations of the thermodynamics of Aβ fibril growth. *Biophys. J.* **96**, 442–452.
20. Małolepsza, E., Boniecki, M., Kolinski, A. & Piela, L. (2005). Theoretical model of prion propagation: a misfolded protein induces misfolding. *Proc. Natl Acad. Sci. USA*, **102**, 7835.
21. Fawzi, N., Okabe, Y., Yap, E. & Head-Gordon, T. (2007). Determining the critical nucleus and mechanism of fibril elongation of the Alzheimer's $A\beta_{1-40}$ peptide. *J. Mol. Biol.* **365**, 535–550.
22. Auer, S., Dobson, C. & Vendruscolo, M. (2007). Characterization of the nucleation barriers for protein aggregation and amyloid formation. *HFSP J.* **1**, 137–146.
23. Liwo, A., Czaplewski, C., Pillardy, J. & Scheraga, H. A. (2001). Cumulant-based expressions for the multibody terms for the correlation between local and electrostatic interactions in the united-residue force field. *J. Chem. Phys.* **115**, 2323–2347.
24. Rojas, A., Liwo, A. & Scheraga, H. (2007). Molecular dynamics with the united-residue force field: ab initio folding simulations of multichain proteins. *J. Phys. Chem. B*, **111**, 293–309.
25. Liwo, A., Arłukowicz, P., Ołdziej, S., Czaplewski, C., Makowski, M. & Scheraga, H. A. (2004). Optimization of the UNRES force field by hierarchical design of the potential-energy landscape: I. Tests of the approach using simple lattice protein models. *J. Phys. Chem. B*, **108**, 16918–16933.
26. Ołdziej, S., Liwo, A., Czaplewski, C., Pillardy, J. & Scheraga, H. A. (2004). Optimization of the UNRES force field by hierarchical design of the potential-energy landscape: II. Off-lattice tests of the method with single proteins. *J. Phys. Chem. B*, **108**, 16934–16949.
27. Ołdziej, S., Łagiewka, J., Liwo, A., Czaplewski, C., Chinchio, M., Nanias, M. & Scheraga, H. A. (2004). Optimization of the UNRES force field by hierarchical design of the potential-energy landscape: III. Use of many proteins in optimization. *J. Phys. Chem. B*, **108**, 16950–16959.
28. Liwo, A., Khalili, M., Czaplewski, C., Kalinowski, S., Oldziej, S., Wachucik, K. & Scheraga, H. (2007). Modification and optimization of the united-residue (UNRES) potential energy function for canonical simulations: I. Temperature dependence of the effective energy function and tests of the optimization method with single training proteins. *J. Phys. Chem. B*, **111**, 260–285.
29. He, Y., Xiao, Y., Liwo, A. & Scheraga, H. (2009). Exploring the parameter space of the coarse-grained UNRES force field by random search: selecting a transferable medium-resolution force field. *J. Comput. Chem.* **30**, 2127–2135.
30. Khalili, M., Liwo, A., Rakowski, F., Grochowski, P. & Scheraga, H. A. (2005). Molecular dynamics with the united-residue (UNRES) model of polypeptide chains: I. Lagrange equations of motion and tests of numerical stability in the microcanonical mode. *J. Phys. Chem. B*, **109**, 13785–13797.
31. Khalili, M., Liwo, A., Jagielska, A. & Scheraga, H. A. (2005). Molecular dynamics with the united-residue (UNRES) model of polypeptide chains: II. Langevin and Berendsen—bath dynamics and tests on model α-helical systems. *J. Phys. Chem. B*, **109**, 13798–13810.
32. Tomaselli, S., Esposito, V., Vangone, P., van Nuland, N., Bonvin, A., Guerrini, R. *et al.* (2006).

The α-to-β conformational transition of Alzheimer's Aβ-(1–42) peptide in aqueous media is reversible: a step by step conformational analysis suggests the location of β conformation seeding. *ChemBioChem*, **7**, 257–267.
33. Lee, J. P., Stimson, E. R., Ghilardi, J. R., Mantyh, P. W., Lu, Y. A., Felix, A. M. *et al.* (1995). H NMR of Aβ amyloid peptide congeners in water solution. Conformational changes correlate with plaque competence. *Biochemistry*, **34**, 5191–5200.
34. Lazo, N. D., Grant, M. A., Condron, M. C., Rigby, A. C. & Teplow, D. B. (2005). On the nucleation of amyloid β-protein monomer folding. *Protein Sci.* **14**, 1581–1596.
35. Barrow, C. J., Yasuda, A., Kenny, P. T. M. & Zagorski, M. G. (1992). Solution conformations and aggregational properties of synthetic amyloid β-peptides of Alzheimer's disease: analysis of circular dichroism spectra. *J. Mol. Biol.* **225**, 1075–1093.
36. Sticht, H., Bayer, P., Willbold, D., Dames, S., Hilbich, C., Beyreuther, K. *et al.* (1995). Structure of amyloid A4-(1–40)-peptide of Alzheimer's disease. *Eur. J. Biochem.* **233**, 293–298.
37. Coles, M., Bicknell, W., Watson, A. A., Fairlie, D. P. & Craik, D. J. (1998). Solution structure of amyloid β-peptide (1–40) in a water–micelle environment. Is the membrane-spanning domain where we think it is? *Biochemistry*, **37**, 11064–11077.
38. Shao, H., Jao, S., Ma, K. & Zagorski, M. (1999). Solution structures of micelle-bound amyloid β-(1–40) and β-(1–42) peptides of Alzheimer's disease. *J. Mol. Biol.* **285**, 755–773.
39. Crescenzi, O., Tomaselli, S., Guerrini, R., Salvadori, S., D'Ursi, A. M., Temussi, P. A. & Picone, D. (2002). Solution structure of the Alzheimer amyloid β-peptide (1–42) in an apolar microenvironment—similarity with a virus fusion domain. *Eur. J. Biochem.* **269**, 5642–5648.
40. Yang, M. & Teplow, D. (2008). Amyloid β-protein monomer folding: free-energy surfaces reveal alloform-specific differences. *J. Mol. Biol.* **384**, 450–464.
41. Anand, P., Nandel, F. & Hansmann, U. (2008). The Alzheimer's β amyloid ($A\beta_{1-39}$) monomer in an implicit solvent. *J. Chem. Phys.* **128**, 165102.
42. Kirkitadze, M. D., Condron, M. M. & Teplow, D. B. (2001). Identification and characterization of key kinetic intermediates in amyloid β-protein fibrillogenesis. *J. Mol. Biol.* **312**, 1103–1119.
43. Fezoui, Y. & Teplow, D. B. (2002). Kinetic studies of amyloid β-protein fibril assembly. Differential effects of α-helix stabilization. *J. Biol. Chem.* **277**, 36948–36954.
44. Koradi, R., Billeter, M. & Wüthrich, K. (1996). MOLMOL: a program for display and analysis of macromolecular structures. *J. Mol. Graphics*, **14**, 51–55.
45. Buchete, N. V., Tycko, R. & Hummer, G. (2005). Molecular dynamics simulations of Alzheimer's β-amyloid protofilaments. *J. Mol. Biol.* **353**, 804–821.
46. Dannenberg, J. (2005). The importance of cooperative interactions and a solid-state paradigm to proteins—what peptide chemists can learn from molecular crystals. *Adv. Protein Chem.* **72**, 227–273.
47. Tsemekhman, K., Goldschmidt, L., Eisenberg, D. & Baker, D. (2007). Cooperative hydrogen bonding in amyloid formation. *Protein Sci.* **16**, 761–764.
48. Plumley, J. & Dannenberg, J. (2010). The importance of hydrogen bonding between the glutamine side chains to the formation of amyloid VQIVYK parallel β-sheets: an ONIOM DFT/AM1 study. *J. Am. Chem. Soc.* **132**, 1758–1759.
49. Tarus, B., Straub, J. E. & Thirumalai, D. (2006). Dynamics of Asp23-Lys28 salt-bridge formation in $A\beta_{10-35}$ monomers. *J. Am. Chem. Soc.* **128**, 16159–16168.
50. Lomakin, A., Chung, D., Benedek, G., Kirschner, D. & Teplow, D. (1996). On the nucleation and growth of amyloid β-protein fibrils: detection of nuclei and quantitation of rate constants. *Proc. Natl Acad. Sci. USA*, **93**, 1125–1129.
51. Harper, J. & Lansbury, P., Jr (1997). Models of amyloid seeding in Alzheimer's disease and scrapie: mechanistic truths and physiological consequences of the time-dependent solubility of amyloid proteins. *Annu. Rev. Biochem.* **66**, 385–407.
52. Naiki, H. & Gejyo, F. (1999). Section II. Characterization of *in vitro* protein deposition: C. Monitoring aggregate growth by dye binding-20. Kinetic analysis of amyloid fibril formation. *Methods Enzymol.* **309**, 305–317.
53. Collins, S., Douglass, A., Vale, R. & Weissman, J. (2004). Mechanism of prion propagation: amyloid growth occurs by monomer addition. *PLOS Biol.* **2**, 1582–1590.
54. Petkova, A., Leapman, R., Guo, Z., Yau, W., Mattson, M. & Tycko, R. (2005). Self-propagating, molecular-level polymorphism in Alzheimer's β-amyloid fibrils. *Science*, **307**, 262–265.
55. Esler, W., Stimson, E., Jennings, J., Vinters, H., Ghilardi, J., Lee, J. *et al.* (2000). Alzheimer's disease amyloid propagation by a template-dependent dock-lock mechanism. *Biochemistry*, **39**, 6288–6295.
56. Cannon, M., Williams, A., Wetzel, R. & Myszka, D. (2004). Kinetic analysis of beta-amyloid fibril elongation. *Anal. Biochem.* **328**, 67–75.
57. García, A. E. & Onuchic, J. N. (2003). Folding a protein in a computer: an atomic description of the folding/unfolding of protein A. *Proc. Natl Acad. Sci. USA*, **100**, 13898–13903.
58. Rhee, Y. M. & Pande, V. S. (2003). Multiplexed-replica exchange molecular dynamics method for protein folding simulation. *Biophys. J.* **84**, 775–786.
59. Andrec, M., Felts, A. K., Gallicchio, E. & Levy, R. M. (2005). Protein folding pathways from replica exchange simulations and a kinetic network model. *Proc. Natl Acad. Sci. USA*, **102**, 6801–6806.
60. García, A. E. & Paschek, D. (2008). Simulation of the pressure and temperature folding/unfolding equilibrium of a small RNA hairpin. *J. Am. Chem. Soc.* **130**, 815–817.
61. Maisuradze, G. G., Senet, P., Czaplewski, C., Liwo, A. & Scheraga, H. A. (2010). Investigation of protein folding by coarse-grained molecular dynamics with the UNRES force field. *J. Phys. Chem. A*, **114**, 4471–4485.

62. Tseng, C., Yu, C. & Lee, H. (2010). From laws of inference to protein folding dynamics. *Phys. Rev. E*, **82**, 021914.
63. Yang, S., Onuchic, J. N., García, A. E. & Levine, H. (2007). Folding time predictions from all-atom replica exchange simulations. *J. Mol. Biol.* **372**, 756–763.
64. Berendsen, H. J. C., Postma, J. P. M., van Gunsteren, W. F., DiNola, A. & Haak, J. R. (1984). Molecular dynamics with coupling to an external bath. *J. Chem. Phys.* **81**, 3684–3690.
65. Späth, H. (1980). *Cluster Analysis Algorithms for Data Reduction and Classification of Objects.* Halsted Press, New York, NY.
66. Ripoll, D. R., Liwo, A. & Scheraga, H. A. (1998). New developments of the electrostatically driven Monte Carlo method—test on the membrane bound portion of melittin. *Biopolymers*, **46**, 117–126.
67. Sugita, Y. & Okamoto, Y. (1999). Replica-exchange molecular dynamics method for protein folding. *Chem. Phys. Lett.* **314**, 141–151.
68. Czaplewski, C., Kalinowski, S., Ołdziej, S., Liwo, A. & Scheraga, H. (2009). Application of multiplexed replica exchange molecular dynamics to the UNRES force field: tests with α and $\alpha+\beta$ proteins. *J. Chem. Theory Comput.* **5**, 627–640.